Density functional study of the pressure tensor for inhomogeneous Lennard–Jones fluids*

Sun Zong-Li(孙宗利)[a)†], Kang Yan-Shuang(康艳霜)[b)], Kang Yan-Mei(康艳梅)[c)], Liu Zhi-Cheng(刘志成)[a)], and Ma Heng-Xin(马恒心)[b)]

[a)] *Science and Technology College, North China Electric Power University, Baoding* 071051, *China*
[b)] *College of Science, Agriculture University of Hebei, Baoding* 071001, *China*
[c)] *Department of Information Science and Technology, University of International Relations, Beijing* 100091, *China*

(Received 23 November 2011; revised manuscript received 3 January 2012)

Based on classical density functional theory, an expression of the pressure tensor for inhomogeneous fluids is presented. This takes into account greater correlation between particles, especially for systems that are geometrically confined or involve an interface. The density and pressure components of Lennard–Jones fluids confined in hard and softened nano-cavities are calculated. A comparison between the results of this work and IK expression suggests that the agreement depends on temperature. The interfacial tension for hard sphere fluids agrees well with the Monte Carlo result when the bulk density is not too large. The results of the solid–fluid interfacial tension for Lennard–Jones fluids demonstrate that different types of external potentials modulate the interfacial tension in different manners.

Keywords: density functional theory, pressure tensor, pair density, interfacial tension

PACS: 61.20.Gy, 62.10.–s **DOI:** 10.1088/1674-1056/21/6/066103

1. Introduction

The pressure tensor $\boldsymbol{P}$ has attracted much attention in both theoretical and experimental fields due to its close relation to capillarity, interfacial phenomena, and hydrodynamics.[1,2] It is of central importance in understanding responses to strain, shear, heat transformation or phase transition. In particular, the thermodynamic properties, such as elastic constant and interfacial tension, also rely on the computation of the pressure tensor. For homogeneous fluids, the pressure p is isotropic and is defined as one-third of the trace of the pressure tensor. However, for inhomogeneous fluids, there is no unique definition because of the arbitrariness of joining the two interacting particles in dealing with the configurational contribution that arises from the pair potential $\varphi(r)$.

Among all the definitions for $\boldsymbol{P}$, the most popular in theoretical formula and computer simulations was originally proposed by Irving and Kirkwood (IK) as follows:[3]

$$\boldsymbol{P} = k_{\mathrm{B}}T\rho(\boldsymbol{r}_1)\boldsymbol{I} - \frac{1}{2}\int \mathrm{d}\boldsymbol{r}_{12}\int_0^1 \mathrm{d}\alpha \frac{\boldsymbol{r}_{12}\boldsymbol{r}_{12}}{r_{12}}\varphi'(r_{12})\rho^{(2)} \times (\boldsymbol{r}_1 - \alpha\boldsymbol{r}_{12}, \boldsymbol{r}_1 + (1-\alpha)\boldsymbol{r}_{12}), \quad (1)$$

in which $\rho^{(2)}(\boldsymbol{r}_1 - \alpha\boldsymbol{r}_{12}, \boldsymbol{r}_1 + (1-\alpha)\boldsymbol{r}_{12})$ denotes the pair density and $\boldsymbol{I}$ the unit tensor. The first term $k_{\mathrm{B}}T\rho(\boldsymbol{r}_1)\boldsymbol{I}$, which can be derived rigorously by calculating the momentum transfer of the particles, is the kinetic contribution of the pressure tensor, and the second term is the configurational counterpart. Much effort has been devoted to the latter.[4–6] From Eq. (1), one can see that the pair density $\rho^{(2)}$, which contains information about the correlation between particles, plays a key role in calculating the pressure tensor. The usual treatment is to perform Taylor expansion in α, and neglect the terms behind the first.[3] However, the exclusion of higher order terms underestimates the correlation between particles and introduces much error, especially for the systems that are geometrically confined or involve an interface. It is therefore necessary to take into account the higher order terms in the expansion of $\rho^{(2)}$ for inhomogeneous systems.

From a general theoretical perspective, one of the most powerful and popular tools for studying inhomogeneous fluids is density functional theory (DFT).[7–9] Despite the lack of knowledge about the exact expression for the excess Helmholtz free energy or the first-order direct correlation function (DCF) of the prac-

*Project supported by the North China Electric Power University Campus Foundation (Grant No. 200911036).
†Corresponding author. E-mail: zongli_sun@163.com
© 2012 Chinese Physical Society and IOP Publishing Ltd

tical system, the density functional approximation (DFA), including functional perturbation expansion approximation (FPEA),[10−12] bridge density functional approximation (BDFA),[13−16] weight density approximation (WDA),[17,18] and fundamental measure theory (FMT),[19] can still be employed with satisfactory performance to study a broad variety of material phenomena for both atomic and colloidal systems.

In particular, the modified version of fundamental measure theory (MFMT)[20] has an important position in the application of DFT in the fields of inhomogeneous fluids.[21−26] Yu *et al.*[21,22] proposed a simple weighted density functional treatment for the attraction based on MFMT for hard core repulsion. The results for the adsorption and phase transition of confined Lennard–Jones (LJ) fluids agree well with Monte Carlo (MC) results. Moreover, in the calculation of interfacial tension, their methodology is superior to Sweatman's treatment, which underestimates interfacial tension for higher bulk density. Fu and Li[23] investigated the excess properties and phase equilibria of confined associating fluids in the framework of MFMT. They observed the interesting phenomenon that there is only one gas–liquid coexistence curve for the hard slit confinement, while two exist for the attractive slit. Yu *et al.*[24] studied the structure and adsorption of confined hard-core multi-Yukawa fluids by using MFMT combined with first-order mean-spherical approximation (FMSA). The capability of describing surface depletion at low temperature indicates the superiority of the DFT approach to those mean-field type theories.

The aim of this paper is to study the pressure tensor of Lennard–Jones fluids confined in nano-cavities within the framework of DFT. Using the well-known relationship: $\boldsymbol{P} = -\boldsymbol{\Pi}$, with $\boldsymbol{\Pi}$ denoting the stress tensor, an alternative expression for $\boldsymbol{P}$ is derived. Our results for the normal pressure $P_{\rm N}$ are compared with those of IK expression, and the difference is discussed in detail. Further, the interfacial tension is calculated based on our derivation. The hard sphere fluids result is compared with that from Monte Carlo simulation.

2. Theory and methods

2.1. Derivation of the expression for $\boldsymbol{P}$

Firstly, choose a closed part with volume $\boldsymbol{G}$ and boundary $\boldsymbol{S}$ arbitrarily from the system. According to the hydrodynamic equation, the force acting on $\boldsymbol{S}$ due to the rate of change of the momentum relates to the stress tensor $\boldsymbol{\Pi}$ via the expression

$$\oint_S \boldsymbol{\Pi}\cdot\boldsymbol{n}\cdot\mathrm{d}\boldsymbol{S} \tag{2}$$

with $\boldsymbol{n}$ denoting the external normal to $\boldsymbol{S}$. Based on the relationship: $\boldsymbol{P} = -\boldsymbol{\Pi}$, one can derive the expression for the pressure tensor by a calculation of $\boldsymbol{\Pi}$. Generally, the rate of change of the momentum of the particles in $\boldsymbol{G}$ consists of two contributions: one is a kinetic contribution, which takes into account the change of momentum owing to the entrance and exit of particles through $\boldsymbol{S}$, while the other considers the inter-particle potential from the particles beyond the volume $\boldsymbol{G}$. Accordingly, $\boldsymbol{\Pi}$ can also be decomposed into the kinetic part and configurational part. The former can be obtained as $-k_{\rm B}T\rho(\boldsymbol{r}_1)\boldsymbol{I}$, while the latter is not uniquely defined because of the arbitrariness of joining the two interacting particles.

To proceed, it is assumed that particle 1 locates in the volume $\mathrm{d}\boldsymbol{r}_1$ at $\boldsymbol{r}_1$ and particle 2 in $\mathrm{d}\boldsymbol{r}_2$ at $\boldsymbol{r}_2$. The force acting on particle 1 due to particle 2 is $-\nabla_1\varphi(|\boldsymbol{r}_1-\boldsymbol{r}_2|)$, then the configurational part of the force acting on the particles in $\boldsymbol{G}$ is given by

$$-\iint \nabla_1\varphi(|\boldsymbol{r}_1-\boldsymbol{r}_2|)\rho^{(2)}(\boldsymbol{r}_1,\boldsymbol{r}_2)\mathrm{d}\boldsymbol{r}_1\mathrm{d}\boldsymbol{r}_2. \tag{3}$$

Defining the relative coordinate $\boldsymbol{r}_{12} = \boldsymbol{r}_1 - \boldsymbol{r}_2$ and coordinate of mass center

$$\boldsymbol{r}_{\rm c} \equiv \frac{\boldsymbol{r}_1+\boldsymbol{r}_2}{2} = \boldsymbol{r}_1 - \frac{1}{2}\boldsymbol{r}_{12},$$

equation (3) can be rewritten as

$$-\int \nabla_1\varphi(r_{12})\mathrm{d}\boldsymbol{r}_{12}\int \rho^{(2)}\left(\boldsymbol{r}_1-\frac{1}{2}\boldsymbol{r}_{12},\boldsymbol{r}_{12}\right)\mathrm{d}\boldsymbol{r}_1 \tag{4}$$

with $r_{12} = |\boldsymbol{r}_{12}|$. Performing a Taylor expansion for $\rho^{(2)}(\boldsymbol{r}_1-\frac{1}{2}\boldsymbol{r}_{12},\boldsymbol{r}_{12})$ about $\rho^{(2)}(\boldsymbol{r}_1,\boldsymbol{r}_{12})$, we have

$$\rho^{(2)}\left(\boldsymbol{r}_1-\frac{1}{2}\boldsymbol{r}_{12},\boldsymbol{r}_{12}\right) = \sum_{n=0}^{\infty}\left(-\frac{1}{2}\boldsymbol{r}_{12}\cdot\nabla_1\right)^n\rho^{(2)}(\boldsymbol{r}_1,\boldsymbol{r}_{12}). \tag{5}$$

In order to understand the correlation between particles, especially when the density of the system varies rapidly, the first three terms are taken into account. Then equation (4) arrives at

$$\begin{aligned}&-\iint \nabla_1\varphi(r_{12})\rho^{(2)}(\boldsymbol{r}_1,\boldsymbol{r}_{12})\mathrm{d}\boldsymbol{r}_{12}\mathrm{d}\boldsymbol{r}_1\\ &+\frac{1}{2}\int \nabla_1\varphi(r_{12})\mathrm{d}\boldsymbol{r}_{12}\int \boldsymbol{r}_{12}\cdot\nabla_1\rho^{(2)}(\boldsymbol{r}_1,\boldsymbol{r}_{12})\mathrm{d}\boldsymbol{r}_1\\ &-\frac{1}{8}\int \nabla_1\varphi(r_{12})\mathrm{d}\boldsymbol{r}_{12}\int(\boldsymbol{r}_{12}\cdot\nabla_1)^2\rho^{(2)}(\boldsymbol{r}_1,\boldsymbol{r}_{12})\mathrm{d}\boldsymbol{r}_1.\end{aligned} \tag{6}$$

The first term equals zero because it expresses the sum of internal forces between particles in the system at equilibrium. Further, by using the Gauss theorem, the second term can be rewritten as

$$\frac{1}{2}\int \nabla_1\varphi(r_{12})\mathrm{d}\boldsymbol{r}_{12}\int \boldsymbol{r}_{12}\cdot\nabla_1\rho^{(2)}(\boldsymbol{r}_1,\boldsymbol{r}_{12})\mathrm{d}\boldsymbol{r}_1 = \frac{1}{2}\int \mathrm{d}\boldsymbol{r}_{12}\nabla_1\varphi(r_{12})\boldsymbol{r}_{12}\oint_S \rho^{(2)}(\boldsymbol{r}_1,\boldsymbol{r}_{12})\boldsymbol{n}\mathrm{d}\boldsymbol{S}. \quad (7)$$

It is noted that the pair density $\rho^{(2)}$ is the diagonal element of the second order density matrix. Accordingly, in the Cartesian coordinates, the terms of $\partial^2/\partial x\partial y$, $\partial^2/\partial y\partial z$, and $\partial^2/\partial z\partial x$ in the third term of Eq. (6) disappear, and only the terms of $\partial^2/\partial x^2$, $\partial^2/\partial y^2$, and $\partial^2/\partial z^2$ remain. Thence, we have

$$\int(\boldsymbol{r}_{12}\cdot\nabla_1)^2\rho^{(2)}(\boldsymbol{r}_1,\boldsymbol{r}_{12})\mathrm{d}\boldsymbol{r}_1 = \sum_{q=x,y,z}\int q_{12}^2\frac{\partial^2\rho^{(2)}}{\partial q_1^2}\mathrm{d}q_1. \quad (8)$$

Using the fact

$$\int q_{12}^2\mathrm{d}\boldsymbol{r}_{12}\int\frac{\partial^2\rho^{(2)}}{\partial q_1^2}\mathrm{d}q_1 = \frac{1}{3}\int r_{12}^2\mathrm{d}\boldsymbol{r}_{12}\int\frac{\partial^2\rho^{(2)}}{\partial q_1^2}\mathrm{d}q_1$$

and the Gauss theorem, we derive the following expression

$$-\frac{1}{8}\int\nabla_1\varphi(r_{12})\mathrm{d}\boldsymbol{r}_{12}\int(\boldsymbol{r}_{12}\cdot\nabla_1)^2\rho^{(2)}(\boldsymbol{r}_1,\boldsymbol{r}_{12})\mathrm{d}\boldsymbol{r}_1 = -\frac{1}{24}\int\nabla_1\varphi(r_{12})r_{12}^2\mathrm{d}\boldsymbol{r}_{12}\oint_S\nabla_1\rho^{(2)}(\boldsymbol{r}_1,\boldsymbol{r}_{12})\boldsymbol{n}\mathrm{d}\boldsymbol{S}. \quad (9)$$

Combining Eqs. (2), (7), and (9), and using the relation $\boldsymbol{P}=-\boldsymbol{\Pi}$, we derive that

$$\boldsymbol{P} = k_\mathrm{B}T\rho(\boldsymbol{r}_1)\boldsymbol{I} - \frac{1}{2}\int\frac{\boldsymbol{r}_{12}\boldsymbol{r}_{12}}{r_{12}}\varphi'(r_{12})\rho^{(2)}(\boldsymbol{r}_1,\boldsymbol{r}_{12})\mathrm{d}\boldsymbol{r}_{12} + \frac{1}{24}\int\frac{\boldsymbol{r}_{12}}{r_{12}}\varphi'(r_{12})r_{12}^2\nabla_1\rho^{(2)}(\boldsymbol{r}_1,\boldsymbol{r}_{12})\mathrm{d}\boldsymbol{r}_{12}. \quad (10)$$

In general conditions, the system may be exposed to an external potential $V_\mathrm{ext}(\boldsymbol{r})$. The presence of $V_\mathrm{ext}(\boldsymbol{r})$ also introduces field-induced contribution to $\boldsymbol{\Pi}$ and then to $\boldsymbol{P}$. Therefore, the pressure tensor becomes

$$\boldsymbol{P} = k_\mathrm{B}T\rho(\boldsymbol{r}_1)\boldsymbol{I} - \frac{1}{2}\int\mathrm{d}\boldsymbol{r}_{12}\frac{\boldsymbol{r}_{12}\boldsymbol{r}_{12}}{r_{12}}\varphi'(r_{12})\rho^{(2)}(\boldsymbol{r}_1,\boldsymbol{r}_{12}) + \frac{1}{24}\int\mathrm{d}\boldsymbol{r}_{12}\frac{\boldsymbol{r}_{12}}{r_{12}}\varphi'(r_{12})r_{12}^2\nabla_1\rho^{(2)}(\boldsymbol{r}_1,\boldsymbol{r}_{12}) + \rho(\boldsymbol{r}_1)\frac{\boldsymbol{r}_1}{r_1}\nabla_1V_\mathrm{ext}(\boldsymbol{r}_1). \quad (11)$$

2.2. Treatment of $\boldsymbol{\rho^{(2)}(r_1, r_{12})}$

It is worthwhile to note that the pair density function $\rho^{(2)}(\boldsymbol{r}_1,\boldsymbol{r}_{12})$ describes the situation when the center of mass of the two-particle pair is at $\boldsymbol{r}_1$, and the separation distance is $\boldsymbol{r}_{12}$. Accordingly, $\rho^{(2)}(\boldsymbol{r}_1,\boldsymbol{r}_{12})$ can generally be rewritten as

$$\rho^{(2)}(\boldsymbol{r}_1,\boldsymbol{r}_{12}) = \rho\left(\boldsymbol{r}_1+\frac{1}{2}\boldsymbol{r}_{12}\right)\times\rho\left(\boldsymbol{r}_1-\frac{1}{2}\boldsymbol{r}_{12}\right)g(r_{12};\tilde{\rho}), \quad (12)$$

where $g(r_{12};\tilde{\rho})$ is a radial distribution function with an average density $\tilde{\rho}$, which is set as the bulk density ρ_b here for simplicity. Assuming that the interparticle potential includes an attractive tail $\varphi_\mathrm{att}(r_{12})$, then $g(r_{12};\tilde{\rho})$ can be given as[27]

$$g(r_{12};\tilde{\rho}) = g^\mathrm{hs}(r_{12};\tilde{\rho})\left[1-\frac{\alpha(\tilde{\rho})\varphi_\mathrm{att}(r_{12})}{k_\mathrm{B}T}\right], \quad (13)$$

where $g^\mathrm{hs}(r_{12};\tilde{\rho})$ is the corresponding radial distribution function of hard sphere fluids,[28] and $\alpha(\tilde{\rho})$ is the compressibility of hard-sphere fluids derived from the Carnahan–Starling equation of state

$$\alpha(\tilde{\rho}) = k_\mathrm{B}T\left(\frac{\partial\tilde{\rho}}{\partial p}\right)_\mathrm{hs} = \frac{(1-\eta)^4}{1+4\eta+4\eta^2-4\eta^3+\eta^4}, \quad (14)$$

where p denotes the bulk pressure and $\eta=\pi d^3\tilde{\rho}/6$ is the packing fraction with the effective hard sphere diameter d.

For simplicity in the computation, Taylor series expansion for the singlet density function $\rho(\boldsymbol{r}_1\pm\frac{1}{2}\boldsymbol{r}_{12})$ about $\boldsymbol{r}_1$ is performed as follows:

$$\rho(\boldsymbol{r}_1\pm\frac{1}{2}\boldsymbol{r}_{12}) = \rho(\boldsymbol{r}_1)\pm\frac{1}{2}\boldsymbol{r}_{12}\cdot\nabla_1\rho(\boldsymbol{r}_1)+\cdots. \quad (15)$$

The density gradient $\nabla_1\rho(\boldsymbol{r}_1)$, representing the total force acting on the particle locating at $\boldsymbol{r}_1$, can be given by the first equation of the Yvon–Born–Green (YBG)[9] hierarchy

$$-k_\mathrm{B}T\nabla_1\ln\rho(\boldsymbol{r}_1) = \nabla_1V_\mathrm{ext}(\boldsymbol{r}_1)+\int\rho(\boldsymbol{r}_2)g(\boldsymbol{r}_1,\boldsymbol{r}_2)\nabla_1\varphi(\boldsymbol{r}_1,\boldsymbol{r}_2)\mathrm{d}\boldsymbol{r}_2. \quad (16)$$

It is easy to find that $\boldsymbol{P}$ can be expressed as a functional of $\rho(\boldsymbol{r}_1)$ and $\nabla_1\rho(\boldsymbol{r}_1)$. Namely, the information about the correlation between particles is included in the terms of $\rho(\boldsymbol{r}_1)$ and $\nabla_1\rho(\boldsymbol{r}_1)$. It is worth noting

that in the bulk phase limit, $\nabla_1\rho(\boldsymbol{r}_1)$ equals zero, and the pressure tensor reduces to the bulk pressure p

$$p = k_{\mathrm{B}}T\rho_b - \frac{2}{3}\pi\rho_b^2\int \varphi'(r_{12})g(r_{12})r_{12}^3\,\mathrm{d}r_{12}, \quad (17)$$

which relates to the structural information alone.

2.3. The DFT for inhomogeneous LJ fluids

According to the classical DFT,[7−9] the grand potential functional $\Omega[\rho(\boldsymbol{r})]$ is formally expressed as

$$\Omega[\rho(\boldsymbol{r})] = \mathscr{F}[\rho(\boldsymbol{r})] + \int \rho(\boldsymbol{r})[V_{\mathrm{ext}}(\boldsymbol{r}) - \mu]\,\mathrm{d}\boldsymbol{r}, \quad (18)$$

where μ is the chemical potential of a particle in the bulk phase and $\mathscr{F}[\rho(\boldsymbol{r})]$ is the intrinsic Helmholtz free energy. As is well known, $\Omega[\rho(\boldsymbol{r})]$ is minimized when the system is at equilibrium, and the equilibrium density profile $\rho(\boldsymbol{r})$ satisfies the variation principle

$$\frac{\delta\Omega[\rho(\boldsymbol{r})]}{\delta\rho(\boldsymbol{r})} = 0. \quad (19)$$

For LJ fluids, the pair potential $\varphi(r) = 4\varepsilon[(r/\sigma)^{12} - (r/\sigma)^6]$ can be split into hard core repulsion $\varphi_{\mathrm{rep}}(r)$ and long ranged attraction $\varphi_{\mathrm{att}}(r)$

$$\varphi_{\mathrm{rep}}(r) = \begin{cases} 4\varepsilon[(r/\sigma)^{12} - (r/\sigma)^6], & r \le \sigma, \\ 0, & r > \sigma; \end{cases} \quad (20)$$

$$\varphi_{\mathrm{att}}(r) = \begin{cases} 0, & r \le \sigma, \\ 4\varepsilon[(r/\sigma)^{12} - (r/\sigma)^6], & r > \sigma; \end{cases} \quad (21)$$

where σ and ε denote, respectively, the diameter of the particle and the strength of the LJ potential.

For non-hard sphere fluids, the most usually employed methodology is to choose the hard sphere fluids as a reference and treat the tails as a perturbation. Thence, the repulsive part defined in Eq. (20) is approximated by the hard sphere potential with the effective diameter d given by[29]

$$d = \frac{1 + 0.2977T^*}{1 + 0.33163T^* + 0.00104771T^{*2}}\sigma. \quad (22)$$

Here, $T^* = k_{\mathrm{B}}T/\varepsilon$ is the reduced temperature. The attractive part in Eq. (21) is treated as perturbation over the reference hard sphere fluids.

Accordingly, $\mathscr{F}[\rho(\boldsymbol{r})]$ can be perturbatively split into ideal gas, hard core repulsion, and long ranged dispersion contributions. That is,

$$\mathscr{F}[\rho(\boldsymbol{r})] = \mathscr{F}_{\mathrm{id}}[\rho(\boldsymbol{r})] + \mathscr{F}_{\mathrm{rep}}[\rho(\boldsymbol{r})] + \mathscr{F}_{\mathrm{att}}[\rho(\boldsymbol{r})]. \quad (23)$$

The ideal gas contribution is exactly known as

$$\mathscr{F}_{\mathrm{id}}[\rho(\boldsymbol{r})] = k_{\mathrm{B}}T\int \rho(\boldsymbol{r})[\ln(\lambda^3\rho(\boldsymbol{r})) - 1]\,\mathrm{d}\boldsymbol{r}$$

with λ denoting the thermal wavelength. However, exact expressions for $\mathscr{F}_{\mathrm{rep}}[\rho(\boldsymbol{r})]$ and $\mathscr{F}_{\mathrm{att}}[\rho(\boldsymbol{r})]$ are unknown for most practical systems. Therefore, approximations for them are necessary to implement the calculations. Among all the DFAs, the MFMT[20] for hard sphere fluids and the analytical result from FMSA[30,31] for long-ranged dispersion have shown a more satisfactory performance in predicting the structure, phenomena transitions, and thermodynamic properties of inhomogeneous fluids. Therefore, in this work, MFMT and FMSA are employed to express $\mathscr{F}_{\mathrm{rep}}[\rho(\boldsymbol{r})]$ and $\mathscr{F}_{\mathrm{att}}[\rho(\boldsymbol{r})]$, respectively. For more details about MFMT and FMSA, refer to the references.

3. Results and discussion

3.1. The equilibrium structure for the inhomogeneous LJ fluids

In order to understand the relationship between the equilibrium structure and the pressure profile, the calculation is initially performed for the density profiles of LJ fluids confined in the spherical cavity. The cavity wall may be hard or softened, which applies, respectively, to the external potential $V_{\mathrm{ext}}^{\mathrm{H}}(r)$ and $V_{\mathrm{ext}}^{\mathrm{S}}(r)$

$$V_{\mathrm{ext}}^{\mathrm{H}}(r) = \begin{cases} 0, & \text{if } r < R, \\ +\infty, & \text{otherwise}, \end{cases} \quad (24)$$

and

$$V_{\mathrm{ext}}^{\mathrm{S}}(r) = \begin{cases} 4\pi\theta\varepsilon_{\mathrm{fs}}\dfrac{R}{r}\left\{\dfrac{\sigma^{12}}{5}\left[\dfrac{1}{(R-r)^{10}} - \dfrac{1}{(R+r)^{10}}\right] - \dfrac{\sigma^6}{2}\left[\dfrac{1}{(R-r)^4} - \dfrac{1}{(R+r)^4}\right]\right\}, & \text{if } r < R, \\ +\infty, & \text{otherwise}. \end{cases} \quad (25)$$

Here R is the radius of the cavity and r is the distance from the center of the cavity. $\varepsilon_{\rm fs}$ in Eq. (25) stands for the strength of the fluid–solid interaction and θ is the number density of atoms on the cavity wall, which is set as $\theta = 1/4\pi$ in all the computation for simplicity.

The numerical results for $\rho(r)$ in different conditions of external potential are plotted in Figs. 1(a) and 1(b). Note that in the computation we choose the reduced bulk density $\rho_{\rm b}^* \equiv \rho_{\rm b}\sigma^3 = 0.6$ and $T^* = 2.5$. The results show that $\rho(r)$ has oscillatory behavior with a period of almost a particle diameter, which indicates the dominance of excluded volume in determining the equilibrium structure. In particular in Fig. 1(b), the oscillation of $\rho(r)$ becomes more pronounced as $\varepsilon_{\rm fs}$ is increased, and in the meanwhile, the soft wall potential has a much more remarkable effect on $\rho(r)$ in the regions near the wall. This effect will be carried through to the pressure tensor, which can be seen in Fig. 3. Actually, according to the first YBG equation, the equilibrium structure is mechanically determined by the competition effect of inter-particle potential and external potential. In other words, the chemical potential of a particle locating at $\boldsymbol{r}$ consists of the intrinsic chemical potential $\mu_{\rm in}(\boldsymbol{r}) = \partial F[\rho(\boldsymbol{r})]/\partial\rho(\boldsymbol{r})$ and the contribution from the external potential, that is, $\mu = \mu_{\rm in}(\boldsymbol{r}) + V_{\rm ext}(\boldsymbol{r})$. Because the field-induced chemical potential increases as $\varepsilon_{\rm fs}$ is increased, the particles tend to shift towards the region where $V_{\rm ext}^{\rm S}(\boldsymbol{r})$ is weaker.

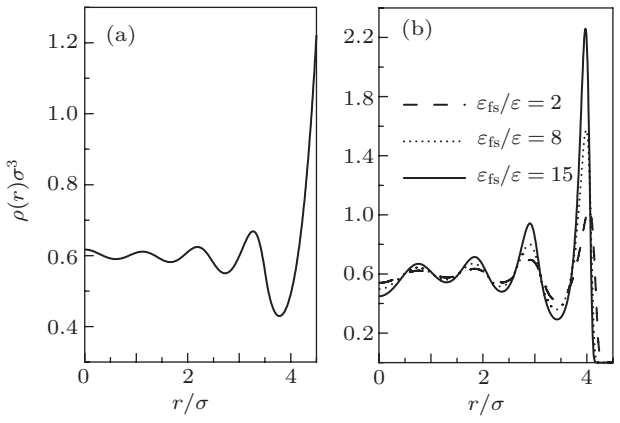


Fig. 1. Density profiles, $\rho(r)$, in conditions of $\rho_{\rm b}^* = 0.6$, $T^* = 2.5$, $R = 5\sigma$. (a) The hard wall condition and (b) the soft wall condition with $\varepsilon_{\rm fs}/\varepsilon = 2, 8, 15$.

3.2. The normal and tangential pressure components

To evaluate the performance of our derivation, the normal and tangential pressure components, $P_{\rm N}(r)$ and $P_{\rm T}(r)$, are calculated for confined LJ fluids. The results in different conditions are plotted, respectively, in Figs. 2–4. By comparing the plots in Figs. 2(a) and 2(b) with those for $\rho(r)$ in Fig. 1, we find that $P_{\rm N}(r)$ oscillates rapidly in the regions where the rapid oscillation in $\rho(r)$ occurs. Further, as shown by the comparison in Figs. 2(a) and 2(b), our results agree well with those of IK, except in the regions near the cavity wall. This is because in these regions, the magnitude of $\nabla\rho(r)$, which is a key quality in determining the pressure, is much larger than that in the inner regions. This will increase the difference between our results and the IK results in the interfacial regions. In addition, our treatment of $\rho^{(2)}(\boldsymbol{r}_1, \boldsymbol{r}_{12})$ in Eq. (12) may introduce errors because this is equivalent to taking $\alpha = 1/2$ in the IK expression. This means that such a rough treatment may ignore some of the correlation between particles, especially in the regions where the density is larger.

Moreover, it is interesting that the comparison between Figs. 2(a) and 2(b) indicates a temperature dependence of the agreement of our results with those of IK. To understand the effect of T^*, we introduce root-mean-square deviation (RMSD) to measure the overall deviation of our results from the IK results

$$\mathrm{RMSD} = \sqrt{\frac{1}{M}\sum_{i=1}^{M}\left(\frac{P_{\rm N}(r_i) - P_{\rm N}^{\rm IK}(r_i)}{P_{\rm N}^{\rm IK}(r_i)}\right)^2}, \quad (26)$$

where M denotes the number of grids divided in the computation and $P_{\rm N}^{\rm IK}$ represents the corresponding IK result. The result for RMSD is plotted in Fig. 2(c). It is obvious that RMSD decreases monotonously with the increase in temperature. This behavior can be explained in terms of the first YBG equation. The magnitude of $\nabla\rho(r)$ decreases with the increase in T^*. This will reduce the difference between the two treatments. In addition, the kinetic contribution of the pressure tensor $k_{\rm B}T\rho(\boldsymbol{r}_1)\boldsymbol{I}$, which is identical in both treatments, plays a more dominant role when the T^* is increased.

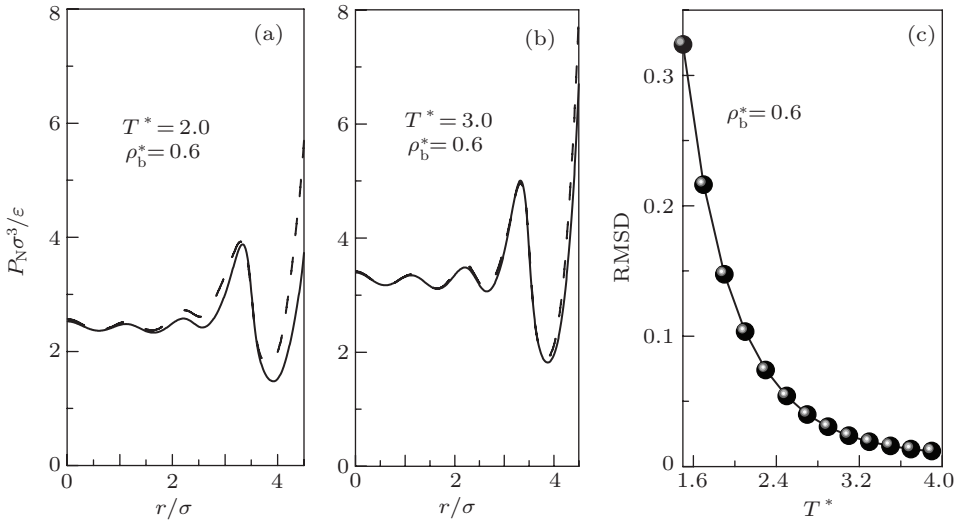


Fig. 2. Comparisons of the $P_N(r)$ of this work (solid line) with that of the IK expression (dashed line) in different conditions of T^* with $\rho_b^*=0.6$ and $R=5\sigma$. Panel (c) illustrates the dependence of RMSD on T^*.

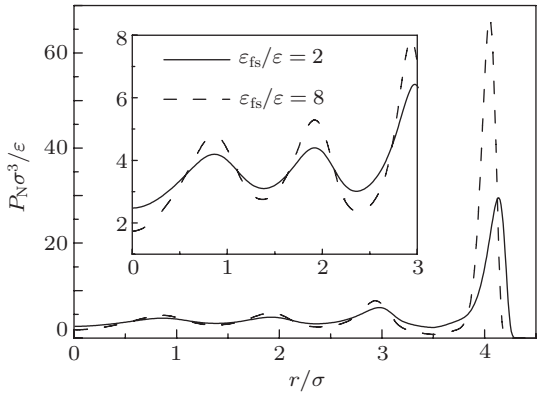


Fig. 3. Profiles of $P_N(r)$ in different conditions of ε_{fs} with $T^*=1.8$, $\rho_b^*=0.6$, and $R=5\sigma$.

Due to the dominance of the external potential in the equilibrium configuration, the pressure tensor in the presence of external potential $V_{ext}^S(\boldsymbol{r})$ may show a considerable difference from that in the absence of $V_{ext}^S(\boldsymbol{r})$ because of its close relation to $\rho(\boldsymbol{r})$. To understand the influence of $V_{ext}^S(\boldsymbol{r})$ on $\boldsymbol{P}$, the calculations for the normal pressure $P_N(r)$ with $\rho_b^*=0.6$, $T^*=1.8$ in the conditions of $\varepsilon_{fs}/\varepsilon=2$ and 8 are performed. The results in Fig. 3 show that in both conditions a peak with large amplitude at 4.0σ exists. Moreover, the height of this peak increases as the fluid–solid interaction becomes stronger. Actually, the profiles of $P_N(r)$ rely closely on the structural and mechanical properties. On the one hand, the kinetics contribution of $P_N(r)$ is proportional to $\rho(r)$, which leads to the value of $P_N(r)$ showing a peak in the position where $\rho(r)$ is at its maximum. On the other hand, in the regions near the peaks of $\rho(r)$, the value of $\nabla\rho(r)$ also has a very large value. On the contrary, in the inner regions, as shown in the inset, the difference between the plots is much smaller because of the weakened influence of $V_{ext}^S(\boldsymbol{r})$ in the regions far from the cavity wall.

To get a comprehensive understanding of the pressure tensor, the tangential pressure $P_T(r)$ for LJ fluids confined in hard and softened cavities is calculated. The results are compared with the normal counterpart in Fig. 4. From the figures, we find that in both conditions, $P_T(r)$ oscillates with almost the same pattern as $P_N(r)$. In the inner regions, the difference between the two components is too small to distinguish, while in the regions near the cavity wall, the difference becomes more apparent because of the large magnitude of $\rho(r)$ and $\nabla\rho(r)$ in these regions.

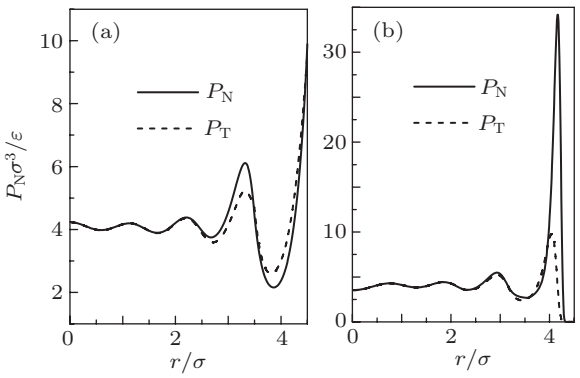


Fig. 4. Comparisons of $P_N(r)$ and $P_T(r)$ in different conditions of external potential with $T^*=3.0$, $\rho_b^*=0.6$, and $R=5\sigma$. Panel (a): the hard wall condition, (b): the softened wall condition with $\varepsilon_{fs}/\varepsilon=2$.

3.3. Solid–fluid interfacial tension from the pressure tensor

The interfacial tension γ is an important quantity of fluids. It reflects the aggregative tendency of particles to minimize the interfacial surface area and the free energy. From the point of view of Virial, γ is defined by the normal and tangential components of the pressure tensor via the expression[1]

$$\gamma = \int \left(\frac{r}{R}\right)^2 [P_{\rm N}(r) - P_{\rm T}(r)] {\rm d}r. \tag{27}$$

To validate our derivation for the pressure tensor, γ for hard sphere fluids near a hard plat wall is calculated. The results are compared with MC simulation results[32] in Fig. 5. It is obvious that our result agrees well with the MC result when the packing fraction is small, while it deviates obviously from the MC result for a larger packing fraction. The disagreement in this case arises mainly from the rough treatment of $\rho^{(2)}(\boldsymbol{r}_1, \boldsymbol{r}_{12})$ in Eq. (12), which leads to the underestimation of γ.

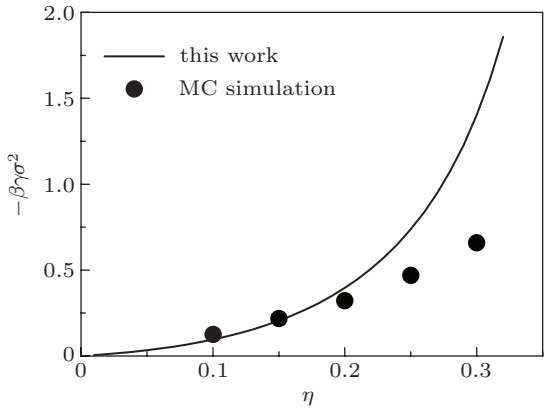


Fig. 5. Interfacial tension for hard sphere fluids near a hard plat wall. Solid line: the result from this work; symbol: the MC simulation result from Ref. [32].

Further, the interfacial tension isotherms for LJ fluids in the case of a hard wall and softened wall are also computed based on our derivation for the pressure tensor. The results are plotted in Figs. 6(a) and 6(b), respectively. Under the condition of the hard wall potential, γ shows a slight increase with $\rho_{\rm b}^*$ when $\rho_{\rm b}^*$ is less than 0.5, while it drops rapidly when $\rho_{\rm b}^*$ is large enough. The increase–decrease transition is the result of the competition between the excluded volume and the dispersion.

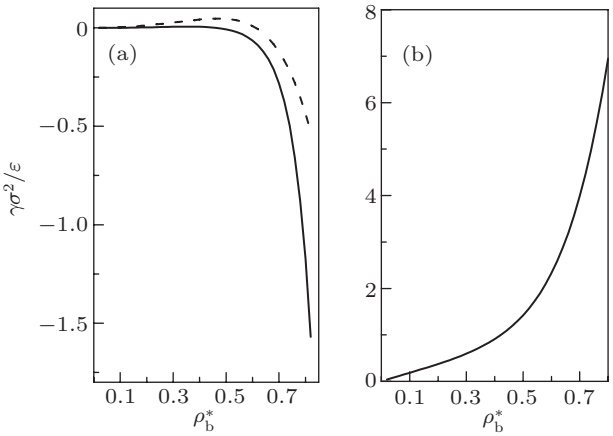


Fig. 6. Interfacial tension isotherms in different conditions of external potential with $T^* = 2.5$ and $R = 5\sigma$: (a) the hard wall condition, and (b) the softened wall condition with $\varepsilon_{\rm fs}/\varepsilon = 2.0$. The solid line is for the results from Eq. (27), and the dashed line for those from Eq. (28).

However, γ increases monotonously with ρ_b^* in the softened wall condition. Moreover, it increases more rapidly when $\rho_{\rm b}^*$ is large enough. This is because the soft potential $V_{\rm ext}^{\rm S}(r)$ excludes the particles to the inner regions, which increases the aggregative tendency of the particles. On the other hand, the rapid decay of density in the region near the wall leads to a reduction in the excluded volume, which is also responsible for the increase in γ. In addition, the dispersion becomes more dominant in its competition with the excluded volume because the peak of $\rho(r)$ locating at 4.0σ becomes higher with the increase in $\rho_{\rm b}^*$. Therefore, the aggregative tendency of the particle in the interface region is greatly increased.

Actually, there are various definitions for interfacial tension. The thermodynamical definition

$$\gamma = \frac{\Omega[\rho(\boldsymbol{r})] + pV}{A} \tag{28}$$

with A and V denoting, respectively, the surface area and volume of the system, is usually employed to predict the solid–fluid interfacial tension because of its convenience in the calculation based on the equilibrium density obtained from DFT. In this work, we have also calculated γ for LJ fluids confined in the hard cavity from Eq. (28), and compared the result with that from Eq. (27). The comparison in Fig. 6(a) shows that γ obtained from both definitions varies with $\rho_{\rm b}^*$ in the same pattern. However, for each $\rho_{\rm b}^*$, γ from Eq. (27) is smaller than that from Eq. (28), especially for the higher bulk density. The underestimation relates to the approximation in the calculation of the pressure components.

4. Conclusion

In summary, an expression for the pressure tensor of inhomogeneous fluids is obtained. This takes into account more of the effects of correlation, especially for systems that are geometrically confined or near a boundary. Our derivation shows that $\boldsymbol{P}$ depends not only on $\rho(r)$, but also on $\nabla\rho(r)$. To perform the calculations of the pressure tensor, the equilibrium structure of confined LJ fluids is initially calculated within the framework of MFMT + FMSA. Further, the pressure components are computed in different cases of external potential. Comparison between the results of this work and those of IK expression suggests that the former agrees qualifiedly well with the latter. In particular, when the wall is softened, both the equilibrium structures and the pressure components are modulated to a great extent due to the influence of $V_{\rm ext}^{\rm S}(r)$, especially in the regions where $V_{\rm ext}^{\rm S}(r)$ is strong. Moreover, a comparison of γ for hard sphere fluids with the MC result shows that there is good agreement when the bulk density is not too large. γ for LJ fluids in the conditions of both hard and soft wall potential gives reliable results. Therefore, despite the approximations in the derivation of the pressure tensor, the present expression for $\boldsymbol{P}$ can predict the pressure and other thermodynamical properties very well. It is hoped that the present methodology might be useful in understanding the hydrodynamics and thermodynamics of fluids at the nanoscale.

References

[1] Rowlinson J S and Widom B 1982 *Molecular Theory of Capillarity* (Oxford: Clarendon Press)

[2] Croxton C A 1986 *Fluid Interfacial Phenomena* (New York: Wiley)

[3] Irving J H and Kirkwood J G 1950 *J. Chem. Phys.* **18** 817

[4] Harasima A 1958 *Adv. Chem. Phys.* **1** 203

[5] Percus J K 1986 *Chem. Phys. Lett.* **123** 311

[6] Todd B D, Evans D J and Daivis P J 1995 *Phys. Rev.* E **52** 1627

[7] Evans R 1979 *Adv. Phys.* **28** 143

[8] Henderson D 1992 *Fundamentals of Inhomogeneous Fluids* (New York: Dekker)

[9] Hansen J P and McDonald I R 1986 *Theory of Simple Liquids* 2nd edn. (New York: Academic)

[10] Ramakrishnan T V and Yussouf M 1979 *Phys. Rev.* B **19** 2775

[11] Calleja M, North A N, Powels J G and Rickayzen G 1991 *Mol. Phys.* **73** 973

[12] Zhou S Q and Ruckenstein E 2000 *Phys. Rev.* E **61** 2704

[13] Zhou S Q and Ruckenstein E 2000 *J. Chem. Phys.* **112** 8079

[14] Choudhury N and Ghosh S K 2001 *J. Chem. Phys.* **114** 8530

[15] Kim S C and Suh S Y 2002 *J. Chem. Phys.* **117** 9880

[16] Zhou S Q 2008 *Chin. Phys.* B **17** 3812

[17] Tarazona P 1985 *Phys. Rev.* A **31** 2672

[18] Denton A R and Ashcroft N W 1985 *Phys. Rev.* A **32** 2909

[19] Rosenfeld Y 1989 *Phys. Rev. Lett.* **63** 980

[20] Yu Y X and Wu J Z 2002 *J. Chem. Phys.* **117** 10156

[21] Yu Y X 2009 *J. Chem. Phys.* **131** 024704

[22] Peng B and Yu Y X 2008 *J. Phys. Chem.* B **112** 15407

[23] Fu D and Li X S 2006 *J. Chem. Phys.* **125** 084716

[24] Yu Y X, You F Q, Tang Y P, Gao G H and Li Y G 2006 *J. Phys. Chem.* B **110** 334

[25] Fu D and Liao T 2007 *Chin. Phys.* **16** 3475

[26] Cao D P, Cheng L S and Wang W C 2007 *Chin. Phys.* **16** 2296

[27] Tang Z X, Scriven L E and Davis H T 1991 *J. Chem. Phys.* **114** 2659

[28] Trokhymchuk A, Nezbeda I, Jirsák J and Henderson D 2005 *J. Chem. Phys.* **123** 024501

[29] Cotterman R L, Schwarz B J and Prausnitz J M 1986 *AIChE J.* **32** 1787

[30] Tang Y P 2003 *J. Chem. Phys.* **118** 4140

[31] Fu D 2006 *J. Chem. Phys.* **124** 164701

[32] Heni M and Löwen H 1999 *Phys. Rev.* E **60** 7057